Journal of Computer-Aided Molecular Design, 11 (1997) 256–264.

J-CAMD 391

Molecular modelling studies of substrate binding to the lipase from *Rhizomucor miehei*

Asutosh T. Yagnik*, Jennifer A. Littlechild and Nicholas J. Turner**

Departments of Chemistry and Biological Sciences, Exeter University, Exeter EX4 4QD, U.K.

Received 23 October 1996
Accepted 26 November 1996

Keywords: Enantioselectivity; Catalytic triad; Protein dynamics; Transition-state complex; Oxazolinones

Summary

Lipase enzymes have found increasingly widespread use, especially in biotransformation reactions in organic synthesis. Due to their efficiency and high enantioselectivity, they can be employed in a variety of reactions to carry out asymmetric hydrolyses, esterifications and transesterifications. However, the reasons for their stereospecificity have not been fully correlated with the enzyme structure. Employing molecular modelling techniques and existing experimental data, a transesterification reaction using *Rhizomucor miehei* lipase was studied. The results indicate that the major controlling factor for this reaction is hydrophobic in nature, providing support for previous literature hypotheses. In addition, computational experiments suggest that the origin of enantioselectivity is the formation of essential hydrogen bonds in and around the catalytic triad of active site residues. Only one enantiomer of the substrate is able to form these hydrogen bonds during the formation of the first tetrahedral transition state.

Introduction

Lipases belong to the group of enzymes generally known as hydrolases (E.C. 3.1.1.3). The term lipase usually refers to triacylglyceride lipases which catalyse the hydrolysis of triacylglycerides, thus liberating fatty acids and glycerols [1]. One of the striking features of lipases is that their activity is greatly increased at a lipid/water interface [2]. This is known as interfacial activation [3,4], where the active site of the enzyme becomes exposed due to the movement of a 'lid' or 'flap' region which normally covers it.

These stable and inexpensive enzymes are known to catalyse asymmetric hydrolyses [5], esterifications and transesterifications [6] of a wide range of substrates. As a result, lipases have found commercial importance as constituents of washing detergents and as catalysts in the synthesis of compounds which serve as precursors to pharmaceuticals, agrochemical and other synthetic targets [7,8]. The lipase from *Rhizomucor miehei* (RML) in the form of Lipozyme®, an immobilised form of the enzyme which is commercially available, has been used to catalyse ring opening of the oxazolin-5(4H)-ones **1**–**3** (Scheme 1), yielding the esters **4**–**6** in varying enantiomeric excess and yields [9]. One of these esters, (*S*)-**1**, was subsequently used in the synthesis of homochiral L-(*S*)-*tert*-leucine, an important amino acid which has found widespread use both as a chiral auxiliary [10,11] and a component of potentially therapeutic pseudopeptides [12].

The catalytic mechanism of RML is believed to be analogous to that proposed for the serine proteases [13–15], involving the known active site triad of residues Ser^{144}, His^{257} and Asp^{203} [3,14]. It has been suggested that a Michaelis–Menten complex (**MM**) (Scheme 2) forms between the substrate and the enzyme [13–15], which proceeds to give the first tetrahedral intermediate ($\mathbf{T_i1}$). This collapses to give an acyl-enzyme intermediate ($\mathbf{AE_i}$), which then forms the second tetrahedral intermediate ($\mathbf{T_i2}$). Finally, the latter breaks down to give the ester product (Scheme 2).

The catalytic triad of residues mediates the reaction via a charge transfer system [15]. During the formation of $\mathbf{T_i1}$, the hydrogen atom of Ser^{144} is transferred to His^{257}

*To whom correspondence should be addressed.
**Present address: Department of Chemistry, University of Edinburgh, King's Buildings, West Mains Road, Edinburgh EH9 3JJ, U.K.

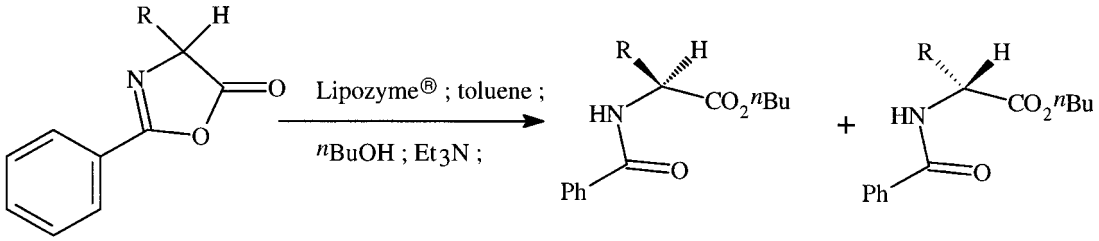

R = *t*-butyl; (±)-**1**

R = CH_2Ph; (±)-**2**

R = *i*-propyl; (±)-**3**

R = *t*-butyl; **4** (99.5% e.e. of *S*-isomer)

R = CH_2Ph; **5** (75.0% e.e. of *S*-isomer)

R = *i*-propyl; **6** (0% e.e.)

Scheme 1. RML catalysed ring opening of oxazolin-5(4H)-ones **1**–**3**, giving the esters **4**–**6** in varying enantiomeric excesses and yields.

and, as the $\mathbf{AE_i}$ is formed, the charged imidazole ring transfers a hydrogen atom to the leaving alcohol group. The $\mathbf{AE_i}$ complex is then cleaved by a nucleophile to give $\mathbf{T_i2}$, in which a hydrogen atom from the protonated His^{257} is transferred to Ser^{144}, thus re-forming the original catalytic centre.

Since the RML-catalysed butanolysis of oxazolinones **1**–**3** exhibits remarkably variable stereospecificity, it was decided to further study the reaction by means of molecular modelling. Specifically, the case where the substrate (±)-**1** was employed was of particular interest, as it gave such a high enantiomeric excess of the ester product (*S*)-**4**. This would allow for a better understanding of the stereospecificity of this enzyme.

Materials and Methods

Molecular modelling equipment

All calculations were performed on Silicon Graphics workstations (Indy PC and Indigo II XL) [16], under the Irix (versions 5.2 and 5.3) operating system. The QUANTA® software (version 4.0) [17] was used for manipulation of molecules, energy minimisation calculations and molecular dynamics simulations. The software employed the CHARMm (version 22.2) force field [18,19]. All calculations were carried out using a distance-dependent dielectric, in order to try and partially compensate for the lack of explicit water molecules (although the crystallographically determined bound water molecules were used), and the default settings of the software, unless otherwise specified.

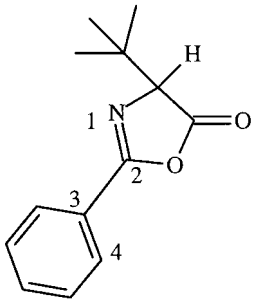

(±)-**1**

Fig. 1. The dihedral angle τ (1,2,3,4), about which a conformational search was performed.

*Modelling of t-butyl oxazolinones (R)- and (S)-**1***

Both isomers of **1** were built and then minimised (with the default dielectric constant of 1) using 100 steps of the steepest descents (SD) algorithm followed by the adopted-basis Newton–Raphson (ABNR) algorithm, until an energy gradient tolerance of 0.001 was satisfied. A conformational search about the dihedral angle τ (1,2,3,4) (Fig. 1) was performed using the Grid Scan method, a systematic conformational searching tool of the software, and a stepwise rotation of 1° increments, between 0° and 180°. During the search, each conformation was minimised using ABNR with the energy gradient tolerance set to 0.001. For each degree scan, the minimised conformation was kept and the grid was kept constrained. Finally, for each enantiomer, the conformation with the lowest energy was selected for use in all further calculations involving the oxazolinones.

The lipase structure

The X-ray coordinates for an enzyme–diethyl phosphate inhibitor complex of RML, with an identifying code of 4TGL [20,21], were obtained from the Brookhaven Protein Databank (PDB) [22].

After importing the PDB file into QUANTA®, the alternate locations were handled as being disordered. The appropriate PATCH file was applied in order to create the disulphide bonds between residues 29–268, 40–43 and

235–244. A separate residue topology file (RTF) was created for the inhibitor molecule. The RTF established the correct molecular topology for the diethyl phosphate inhibitor molecule and contained all the information necessary for other calculations. This gave structure **A**, which was used as a basis from which to create the other structures.

Since the enzyme–inhibitor structure, **A**, was known to mimic the $\mathbf{T_i1}$ complex [13] (Scheme 2), the His^{257} residue was changed from type HIS (normal histidine residue) to HSC (protonated histidine residue) in order to correctly represent the hydrogen bonding that would be expected in the active site area. A covalent bond was created between the Ser^{144} oxygen atom and the phosphorus atom of the inhibitor, and an RTF for this new residue was created. To the resulting structure, **B**, were added all the hydrogen atoms. The hydrogen atom positions of **B** were optimised by minimising only the hydrogen atoms, whilst keeping all the other atoms fixed. The procedure used 100 steps of SD followed by ABNR until an energy gradient

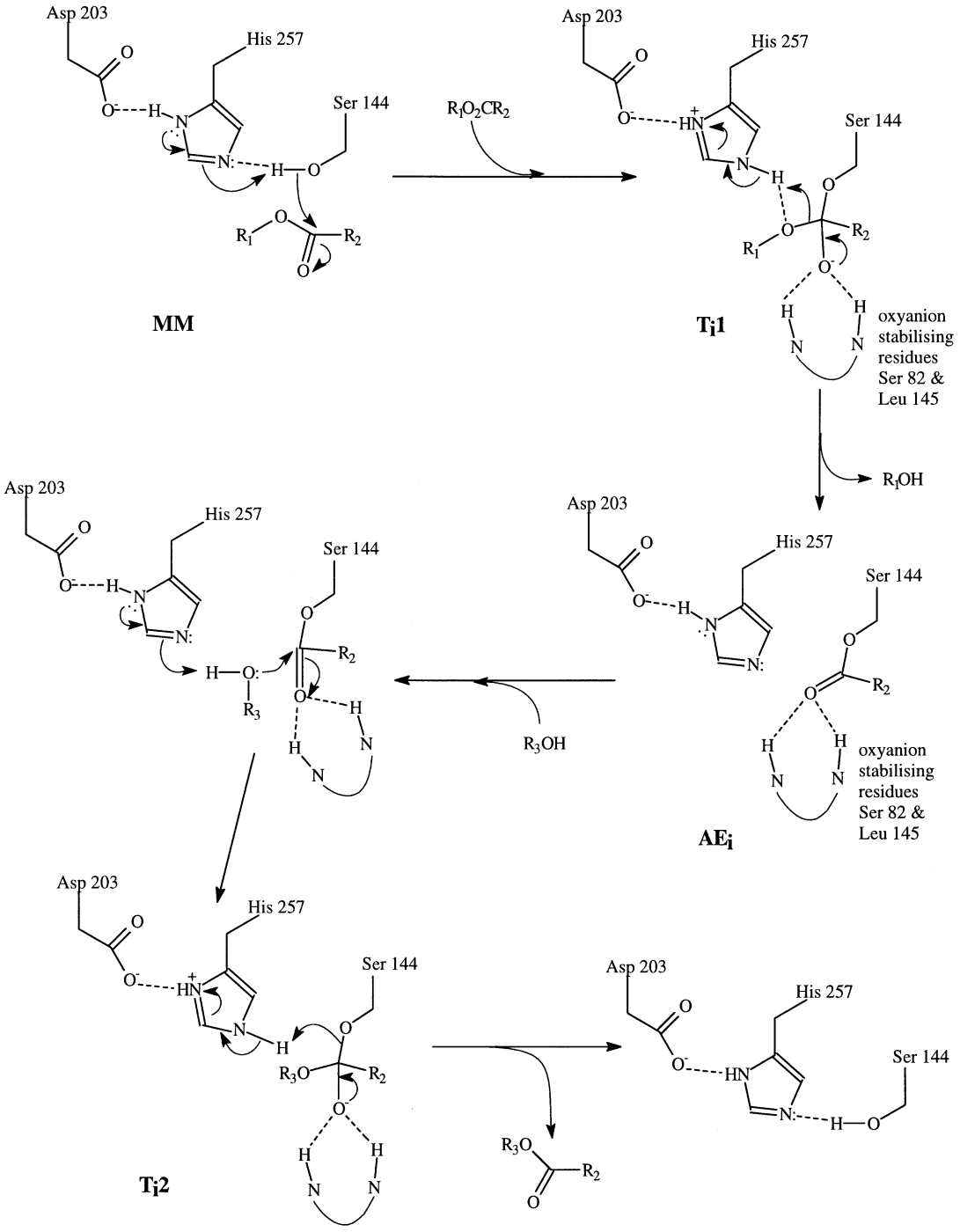

Scheme 2. Suggested catalytic mechanism of RML, analogous to that proposed for the serine proteases [13–15].

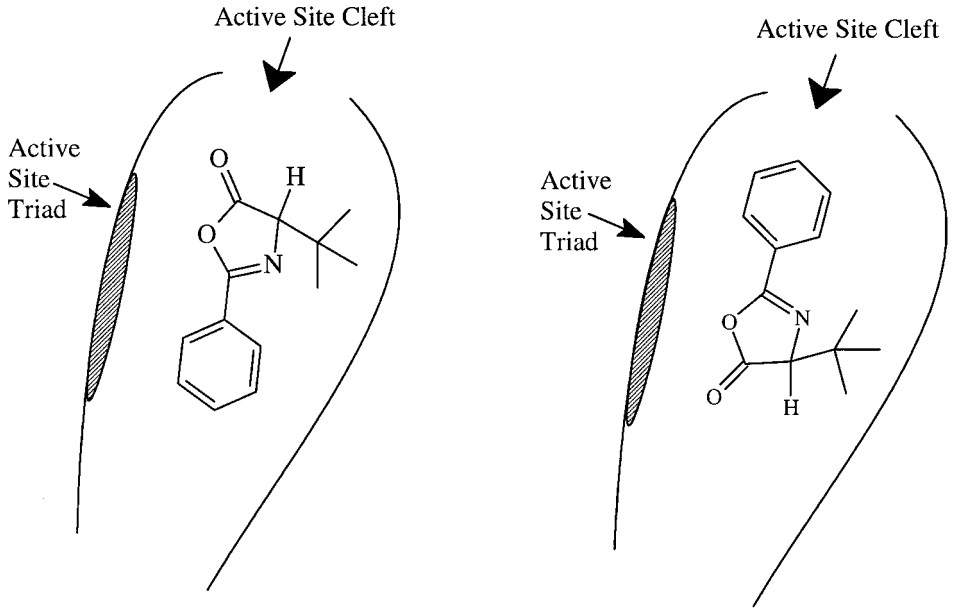

C-(*R*)-**1**(**i**) & **C**-(*S*)-**1**(**i**)
(Placed in active site according to probe calculation results).

C-(*R*)-**1**(**ii**) & **C**-(*S*)-**1**(**ii**)
(Placed in opposite orientation to that suggested by probe calculations).

Fig. 2. Diagrammatic representation of the two possible orientations of both (*R*)- and (*S*)-**1** in the active site of the enzyme.

tolerance of 0.01 was satisfied. This model was used as a control, before progressing to using the methodology with other models. In all protein minimisations, a distance-dependent dielectric was used together with default settings for the other parameters.

Another structure of 4TGL, **C**, was created from **A** by removing the inhibitor but retaining His^{257} as residue type HIS. The hydrogen atom positions of **C** were optimised using the same method as for **B**. This model was used to test the feasibility of the reaction by assessing whether the compounds (*R*)- and (*S*)-**1** would form **MM** complexes with the enzyme. Probe calculations on all residues within a 12 Å sphere from Ser^{144} were carried out on **C** using both the electrostatic and van der Waals terms. Benzene and methyl propane molecules were used as the probes, in order to most accurately represent the major substituents attached to the oxazolinone ring of compounds (*R*)- and (*S*)-**1**. In addition, solvent accessibility calculations within QUANTA, using both water and *n*-butanol molecules, were carried out in the same region of **C**.

Structure **D** was similar to **B** in that the His^{257} residue type was represented as HSC, but as for **C**, the inhibitor

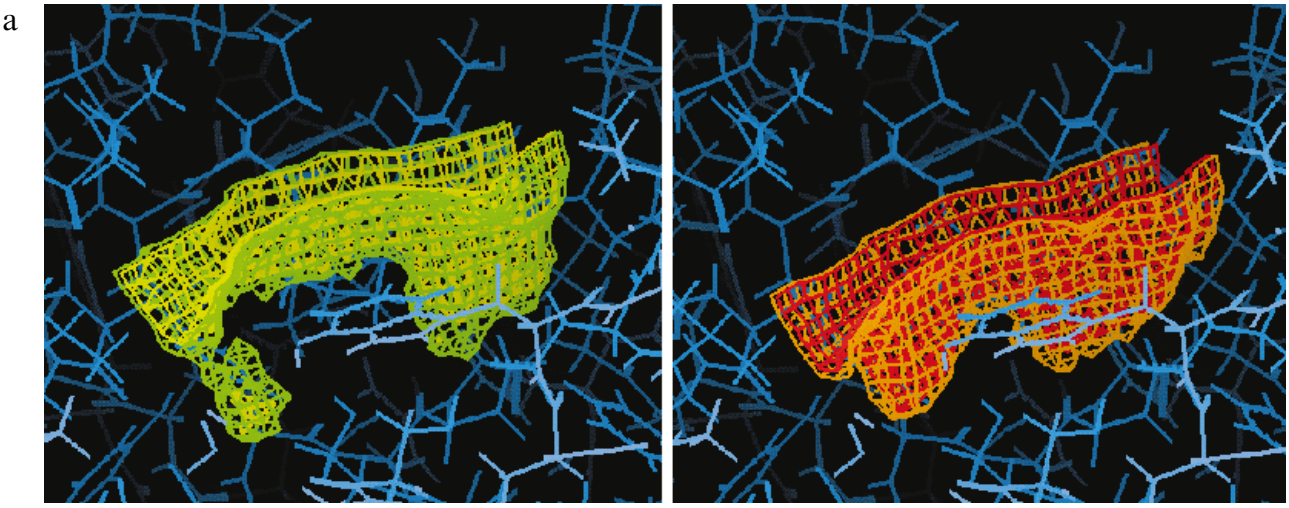

Fig. 3. Results of probe calculation on **C**, indicating the preferred region where (a) a *t*-butyl group and (b) a benzyl group could be accommodated.

TABLE 1
DIFFERENT PROTEIN STRUCTURES **A**, **B**, **C**-(*R*)-**1(i)**, **C**-(*S*)-**1(i)**, **C**-(*R*)-**1(ii)**, **C**-(*S*)-**1(ii)**, **D**-(*R*)-**1(i)** AND **D**-(*S*)-**1(i)**

Structures	Brief description
A	Initial PDB file imported into QUANTA, correct symmetry and space group assigned. Appropriate PATCH file applied to create disulphide bridges. Correct molecular topologies established for inhibitor and rest of protein. Used as a starting point to create other structures by editing residue types and atom charges as necessary.
B	Used as a control. Inhibitor retained and protein–inhibitor complex mimicking $\mathbf{T_i1}$ complex created, with correct atom charges and residue types. Minimisations carried out on the hydrogen atoms to test method and make sure it would not adversely affect the protein structure.
C-(*R*)- and (*S*)-**1(i)** and **C**-(*R*)- and (*S*)-**1(ii)**	Inhibitor removed and in its place were docked (*R*)- and (*S*)-**1(i)** and (*R*)- and (*S*)-**1(ii)**. Model used to test feasibility of whether substrates would form **MM** type complexes. Minimisations carried out and results, together with those from probe calculations, provided an indication of preferred binding orientation of substrates.
D-(*R*)-**1(i)** and **D**-(*S*)-**1(i)**	Similar to structure **B**. However, in this case the inhibitor was removed and protein–substrate complexes mimicking the $\mathbf{T_i1}$ transition state created for (*R*)- and (*S*)-**1(i)**. Minimisations followed by dynamics simulation carried out in order to determine which of the enantiomers was computationally preferred, during the RML-catalysed biotransformation reaction described in Scheme 1.

was removed. Using the previous methodology, all the hydrogen atoms were added to the structure and their positions optimised. This was carried out to simulate the $\mathbf{T_i1}$ complex that may form between the enzyme and one of the substrates (*R*)- and (*S*)-**1**. The structures **A**, **B**, **C** and **D** are summarised in Table 1.

Investigation of the Michaelis–Menten complex

Possible binding modes of the substrate with 4TGL were investigated by manually docking the substrates (*R*)- and (*S*)-**1(i)** into the active site of **C** (structures **C**-(*R*)-**1(i)** and **C**-(*S*)-**1(i)**, Fig. 2). The probe results from **C** were used as a guide as to where the *t*-butyl and benzyl groups should lie. The position of the diethyl phosphate inhibitor in **B** was also used as a guide when placing the substrates in the active site. The carbonyl carbon atom of the oxazolinone ring was overlaid with the phosphorus atom of the inhibitor, together with the corresponding oxygen atoms. After placing the substrates in the active site of **C**, a minimisation was carried out using 100 steps of SD followed by ABNR until an energy gradient tolerance of 0.01 was satisfied. All residues within a 12 Å sphere from the Ser^{144} were allowed to move freely and a harmonic constraint force of 100 was placed on the rest of the structure.

Opposite orientations of both isomers of the substrate, (*R*)- and (*S*)-**1(ii)**, to those suggested by the probe calculations were also manually docked into the active site of **C** (structures **C**-(*R*)-**1(ii)** and **C**-(*S*)-**1(ii)**, Fig. 2) using the same methodology.

Investigation of the first tetrahedral intermediate $\mathbf{T_i1}$: Possible modes of substrate binding

A surface calculation was carried out on **D**, using a probe radius of 1.0 Å, to obtain an idea of the overall shape and size of the active site cleft. Following this, both isomers of the substrate (*R*)- and (*S*)-**1(i)** were placed one at a time into the active site of **D** using, as before, the position of the inhibitor atoms as a guide. The position of the carbonyl oxygen atom was checked to ensure that it formed hydrogen bonds with both of the oxyanion stabilising residues, Ser^{82} and Leu^{145}, as described in the literature [3,14]. A covalent bond was created between the Ser^{144} oxygen atom and the carbonyl carbon atom of the oxazolinone ring. The carbonyl oxygen atom type was changed to OC, representing a charged oxygen atom species, and given a formal point charge of –1. This gave two tetrahedral intermediate ($\mathbf{T_i1}$) complexes, structures **D**-(*R*)-**1(i)** and **D**-(*S*)-**1(i)**, representing both isomers of the oxazolinone substrates. Minimisation of each of these was carried out using 100 steps of SD followed by ABNR until an energy gradient tolerance of 0.01 was satisfied. All residues within a 12 Å sphere from the Ser^{144} were allowed to move freely and a harmonic constraint force of 100 was placed on the rest of the structure.

Molecular dynamics simulation of the first tetrahedral intermediates

The minimised structures **D**-(*R*)-**1(i)** and **D**-(*S*)-**1(i)** were used in order to carry out molecular dynamics simulations of these tetrahedral intermediates $\mathbf{T_i1}$. The dynamics involved heating the systems from 0 to 300 K during 0.3 ps, followed by equilibration during 0.3 ps and finally simulation during 0.6 ps. As for the minimisations, residues within a 12 Å sphere from the Ser^{144} were allowed to move freely and a harmonic constraint force of 100 was placed on the rest of the structure. The heating was started from the beginning and the equilibration and simulation from the restart files. The whole dynamics calculation was run with the SHAKE option on and using a distance-dependent dielectric. After the dynamics run had been completed, a total CHARMm energy was calculated (with constraints still applied) and the intramolecular interactions were examined. Using the Analysis tool within QUANTA, the dynamics trajectories were replayed as animation files with corresponding energy plots. These were visually analysed to investigate the overall motions of the structures, particularly in the region of the active site.

Results

*Structure **B***

The addition of all hydrogen atoms to **B**, followed by subsequent minimisation in order to optimise their positions, was used as a control in the experiment. The rms difference, excluding hydrogen atoms, between the initial and minimised structures was 0.42. This result showed that our proposed method for subsequent calculations was viable since the overall structure was not significantly affected. It was possible to create the $\mathbf{T_i1}$ transition state which the 4TGL enzyme–inhibitor complex represented and thus establish the correct atom types, bonding and charges that should be present in the active site region.

*Structure **C**: The Michaelis–Menten complexes*

The probe calculations on **C**, including all the hydrogen atoms, indicated there to be a preferred region where a *t*-butyl group could be accommodated (Fig. 3a), whereas that for the benzene group was not as clear (Fig. 3b). This qualitative result indicated that the preferred location of the substrates in the active site of **C** would decrease in the order (*S*)-**1(i)** > (*R*)-**1(i)** > (*R*)-**1(ii)** > (*S*)-**1(ii)**. The solvent accessibility calculations showed, as expected, that the active site cleft of the enzyme was very exposed to solvent, but more so to water molecules than to *n*-butanol.

Minimisation of each of the enzyme–substrate **MM** complexes showed **C**-(*R*)-**1(ii)** to have the lowest relative energy and, together with **C**-(*S*)-**1(ii)**, also the largest rmsd from the initial structure. The second lowest energy and lowest rmsd was found with structure **C**-(*S*)-**1(i)**. The results (energy values quoted to show relative differences) are summarised in Table 2.

A closer examination of the active site though showed that only substrates **C**-(*R*)-**1(i)** and **C**-(*S*)-**1(i)** had maintained a favourable position which would allow for subsequent nucleophilic attack by the Ser^{144} oxygen atom on the carbonyl carbon atom of the oxazolinone. In addition, this conformation of the substrate allowed for stabilising hydrogen bonding, in the oxyanion hole, between the carbonyl oxygen atom of the oxazolinone and the NH groups of Leu^{145} and Ser^{82} (Figs. 4a and b). For the other structures **C**-(*R*)-**1(ii)** and **C**-(*S*)-**1(ii)**, although the substrates had shifted into energetically favourable positions, these did not allow for the correct **MM** conformation needed in the vicinity of the active site for catalysis to proceed (Figs. 5a and b).

*Structure **D**: The first tetrahedral intermediate $\mathbf{T_i1}$*

The acyl-enzyme intermediate structures, **D**-(*R*)-**1(i)** and **D**-(*S*)-**1(i)**, mimicking the $\mathbf{T_i1}$ complex were built. Minimisation showed **D**-(*S*)-**1(i)** to have an energy 6.2 kcal mol^{-1} lower than that of **D**-(*R*)-**1(i)**. The *t*-butyl groups of both (*R*)- and (*S*)-**1(i)** had adopted similar positions in the active site. In both **D**-(*R*)-**1(i)** and **D**-(*S*)-**1(i)**, the oxyanions of the $\mathbf{T_i1}$ complexes were stabilised by hydrogen bonding with the NH groups of Ser^{82} and Leu^{145}. In addition, hydrogen bonding occurred between the oxygen atom of the oxazolinone ring and the NH group of His^{257}.

A molecular dynamics simulation of both structures supported the findings of the minimisations. In **D**-(*R*)-**1(i)**, the oxyanion formed a hydrogen bond with the NH group of Ser^{82} and with the OH group of Tyr^{28} (Fig. 6a). There was also no hydrogen bonding between the catalytic residues Asp^{203} and His^{257} (Fig. 6a). However, in **D**-(*S*)-**1(i)** all the original hydrogen bonding was still present (Fig. 6b). The total energies of both structures showed that of **D**-(*S*)-**1(i)** to be 4.8 kcal mol^{-1} lower than **D**-(*R*)-**1(i)**.

Overlaying results from the surface calculation on **D** onto the coordinates of **D**-(*S*)-**1(ii)** showed the *t*-butyl group to lie in a large hydrophobic 'pocket' of similar size (Fig. 7).

Discussion

The solvent accessibility calculations helped to explain why it is so important to carry out esterification/transesterification reactions in a dry environment, since any water would lead to the competing hydrolysis reaction taking place and formation of the corresponding carboxylic acid.

Although the probe calculations indicated that the substrates were more likely to fit into the active site in one orientation, the **MM** complex formation was investigated for both orientations. This was done to show the validity of the probe calculations as well as to ascertain whether the reaction was able to proceed through to the next stage of catalysis, or whether the substrates would be rejected from the active site.

Minimisation of the **MM** complexes **C**-(*R*)-**1(i)**, **C**-(*S*)-**1(i)**, **C**-(*R*)-**1(ii)** and **C**-(*S*)-**1(ii)** showed that only the substrates in **C**-(*R*)-**1(i)** (Fig. 4a) and **C**-(*S*)-**1(i)** (Fig. 4b) had maintained a favourable position, which would allow for the enzyme catalysis to proceed. Although structures **C**-(*R*)-**1(ii)** (Fig. 5a) and **C**-(*S*)-**1(ii)** (Fig. 5b) had relatively favourable energies of minimisation (Table 2), the substrates (*R*)- and (*S*)-**1(ii)** had been shifted so as to no

TABLE 2
DIFFERENCES IN RELATIVE ENERGY AND RMSD VALUES BETWEEN THE **MM** COMPLEXES **C**-(*R*)-**1(i)**, **C**-(*S*)-**1(i)**, **C**-(*R*)-**1(ii)** AND **C**-(*R*)-**1(ii)** (SEE FIG. 2)

MM complex	Minimised energy (kcal mol^{-1})	Rmsd from initial structure
C-(*R*)-**1(i)**	−3277	0.34
C-(*S*)-**1(i)**	−3305	0.28
C-(*R*)-**1(ii)**	−3319	0.41
C-(*S*)-**1(ii)**	−3296	0.37

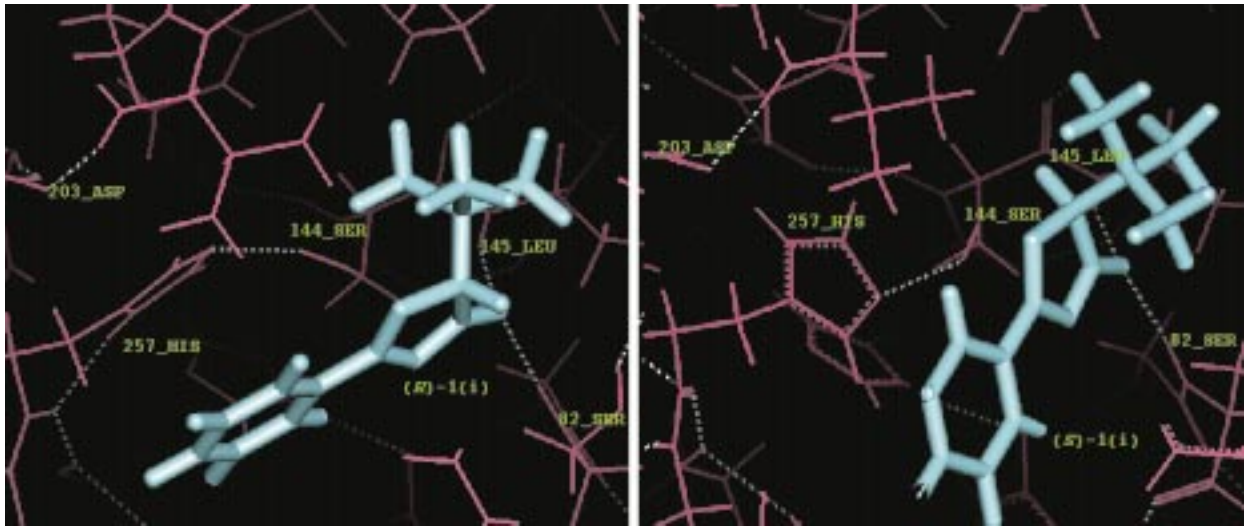

Fig. 4. Structure **C**-(*R*)-**1**(**i**) (a) and structure **C**-(*S*)-**1**(**i**) (b) are stabilised by hydrogen bonding in the 'oxyanion hole'. (a) The oxazolinone (*R*)-**1**(**i**) is in a favourable position for nucleophilic attack by the oxygen atom of nearby Ser^{144}. (b) The oxazolinone (*S*)-**1**(**i**) is in a favourable position for nucleophilic attack by the oxygen atom of nearby Ser^{144}, but more so than with (*R*)-**1**(**i**).

longer allow for the correct **MM** position necessary for catalysis to proceed.

Since (*R*)- and (*S*)-**1**(**i**) were shown to adopt the most favourable **MM** positions, it was decided to use only these when studying the first tetrahedral intermediate complex $\mathbf{T_i1}$. The lower minimised energy of **D**-(*S*)-**1**(**i**) suggested that the (*S*)-isomer of the oxazolinone would be more favoured for catalysis and therefore agreed with the experimental results. Similarly, the difference in CHARMm energies of **D**-(*R*)-**1**(**i**) and **D**-(*S*)-**1**(**i**) calculated after the dynamics simulations, although not being as great, suggested the same. The differences in energies become more meaningful when considering a Boltzmann distribution of the energy difference versus the more prevalent isomer. This shows that at an energy difference of 4.1 kcal mol^{-1}, 99.9% of one isomer would be expected to predominate.

Mapping the surface of **D** onto the results from the dynamics simulation showed a hydrophobic region of the enzyme to be of almost the same size as the large *t*-butyl group of the substrate. It is believed that, in attempting to accommodate the *t*-butyl group of **D**-(*R*)-**1**(**i**) into a predominantly hydrophobic region, conformational changes occurred in the region of the active site that increased certain interresidue distances and, therefore, essential hydrogen bonding could not take place. This was not the case for **D**-(*S*)-**1**(**i**), where the correct stereochemistry at the chiral carbon atom in the oxazolinone ring meant that it was more facile to accommodate the *t*-butyl group into the hydrophobic pocket, with minimal overall change in

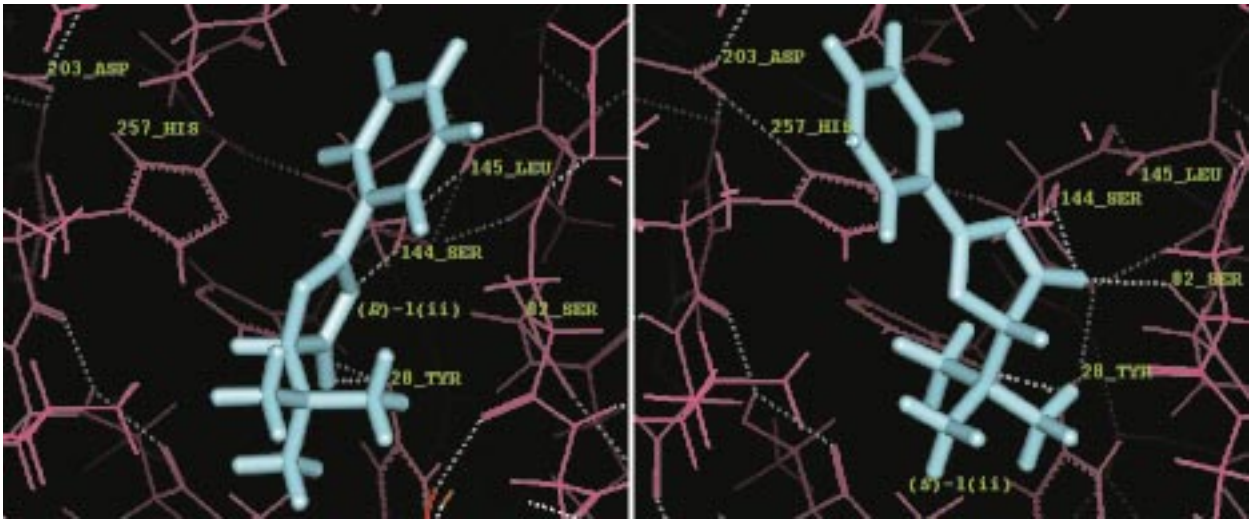

Fig. 5. Structure **C**-(*R*)-**1**(**ii**) (a) and structure **C**-(*S*)-**1**(**ii**) (b) in an energetically unfavourable position which does not allow the correct **MM** conformation in the active site for catalysis to proceed.

a

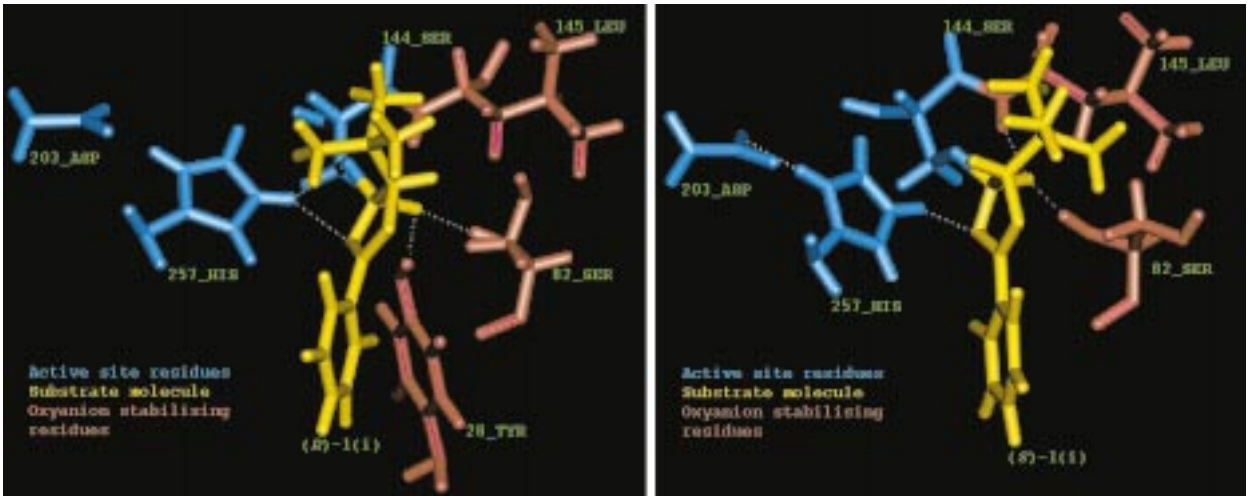

b

Fig. 6. (a) After a molecular dynamics simulation, the oxyanion in **D**-(*R*)-**1(i)** formed a hydrogen bond with the NH group of Ser[82] and the OH group of Tyr[28]. No hydrogen bonding is present between the catalytic residues Asp[203] and His[257]. (b) After a molecular dynamics simulation, the oxyanion in **D**-(*S*)-**1(i)** formed a hydrogen bond with the NH groups of Ser[82] and Leu[145]. The necessary hydrogen bonding between the catalytic residues Asp[203] and His[257] is also present.

conformation in the active site. In other words, it is believed that the predominant controlling factor of the reaction lies primarily in accommodating the bulky hydrophobic groups first. This hypothesis would also explain the differing enantiomeric excesses of the ester products (Scheme 1). For example, in the case where the *t*-butyl group was replaced by an *i*-propyl group, the enantiomeric excess dropped to zero. It seems quite likely that the smaller substituent at the 4-position of the oxazolinone ring makes the formation of $\mathbf{T_i1}$ easier for both enantiomers, thus allowing the correct bonding and conformation to be present in both cases.

Ways ahead

Thus far, the work has pointed to reasons why the *S*-isomer of **1** is the preferred enantiomer for butanolysis using RML. However, it would be more useful to study the system using longer dynamics simulation times. It is

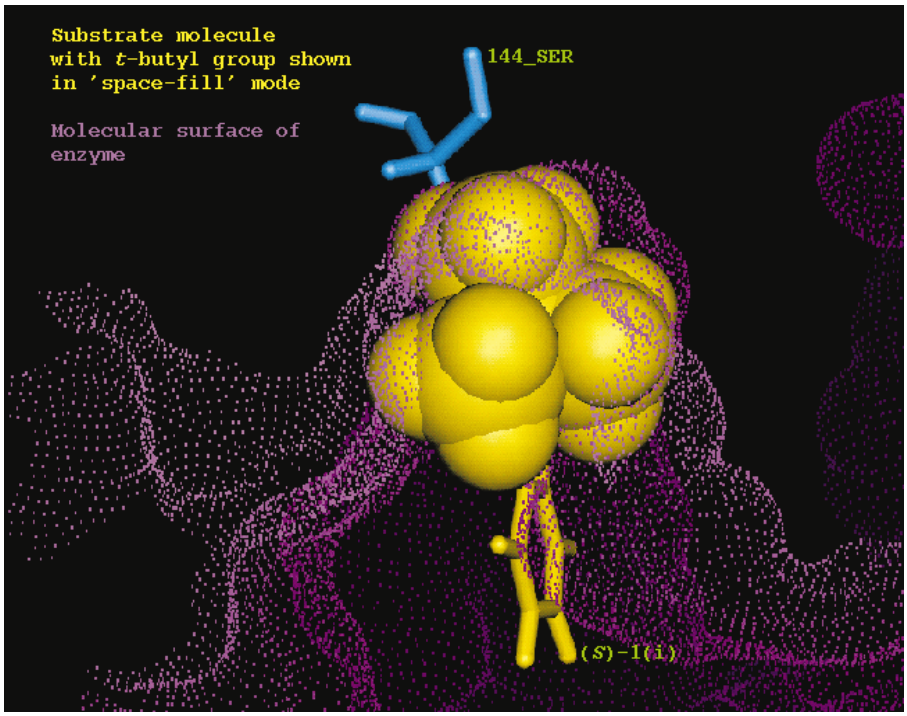

Fig. 7. Overlaying the results of a molecular surface calculation on **D** with the coordinates of **D**-(*S*)-**1(i)** clearly shows the *t*-butyl group of the oxazolinone (*S*)-**1(i)** to lie in a hydrophobic pocket of similar size and shape.

proposed to extend this study to include the cases where benzyl and *i*-propyl groups were used in the oxazolinone ring instead of *t*-butyl. In this way, it may be possible to determine why the enantiomeric excess of the ester product (*S*)-**4** was so high compared to the other esters (*S*)-**5** and (*S*)-**6**. In addition, it would be of interest to synthesise phosphorus-containing inhibitors which could mimic the $\mathbf{T_i1}$ transition state for the oxazolinones. It is hoped that a subsequent X-ray analysis of such an enzyme–inhibitor complex would provide experimental evidence to support this hypothesis.

Conclusions

The current study has helped to gain an insight into why a previously reported *Rhizomucor miehei* lipase catalysed transesterification of the oxazolin-5(4H)-one **1** (Scheme 1) [9] was highly stereospecific for the (*S*)-isomer. The reaction was studied using molecular modelling techniques, together with a suggested catalytic mechanism (Scheme 2). Firstly, an area around the active site, as ascertained from the X-ray crystallographic coordinates of 4TGL [21], was mapped out using benzene and methyl propane probe molecules. The resulting preferred binding areas were used as a guide when studying which orientation the substrate would bind in (see Fig. 2). Four **MM** intermediates were constructed, **C**-(*R*)- and (*S*)-**1(i)** as well as **C**-(*R*)- and (*S*)-**1(ii)** (Table 1), two orientations for each stereoisomer of **1**. Minimisation of these showed only structures **C**-(*R*)- and (*S*)-**1(i)** to retain the correct conformation in the vicinity of the active site for the formation of an **MM**-type complex and thus allow the reaction to progress.

Two structures mimicking the first tetrahedral intermediate $\mathbf{T_i1}$, **D**-(*R*)- and (*S*)-**1(i)**, were subsequently created and studied using minimisation and molecular dynamics. The final structures were found to have an energy difference of 4.8 kcal mol^{-1}, in favour of **D**-(*S*)-**1(i)**. More importantly though, examination around the active site showed only the latter structure to retain the hydrogen bonding network necessary for the reaction to proceed, making it the more easily accessible and thus preferred stereoisomer of the two. This was in agreement with the experimental results [9]. Finally, solvent accessibility calculations showed the active site to be more exposed to water molecules than those of *n*-butanol, helping to explain why 'dry' conditions are so important for such reactions in organic media, if one is to prevent the competing hydrolysis reaction.

References

1 Brockman, H.L., In Borgstroem, B. and Brockman, H.L. (Eds.) Lipases, Elsevier, Amsterdam, The Netherlands, 1984, pp. 4–46.
2 Peterson, W.A., Vidal, J.C., Volwerk, J.J. and De Haas, G.H., Biochemistry, 13 (1974) 1455.
3 Brozozowski, A.M., Derewenda, U., Derewenda, Z.S., Dodson, G.G., Lawson, D.M., Turkenburg, J.P., Bjorkling, F., Huge-Jensen, B., Patkar, S.A. and Thim, L., Nature, 351 (1991) 491.
4 Dodson, G.G. and Lawson, D.M., Faraday Discuss. Chem. Soc., 3 (1992) 1.
5 Ladner, W.E. and Whitesides, G.M., J. Am. Chem. Soc., 106 (1984) 7250.
6 Wang, Y.-F. and Wong, C.-H., J. Org. Chem., 53 (1988) 3127.
7 Crout, D.H.G. and Christen, M., In Scheffold, R. (Ed.) Modern Synthetic Methods, Vol. 5, Springer, Berlin, Germany, 1989, pp. 1–114.
8 Santaniello, E., Ferraboschi, P., Grisenti, P. and Manzocchi, A., Chem. Rev., 92 (1992) 1071.
9 Turner, N.J., Winterman, J.R., McCague, R., Parratt, J.S. and Taylor, S.J.C., Tetrahedron Lett., 36 (1995) 1113.
10 Behnen, W., Dauelsberg, C.H., Wallbaum, S. and Martens, J., Synth. Commun., 22 (1992) 2143.
11 Hashimoto, S.I. and Koga, K., Chem. Pharm. Bull., 27 (1979) 2760.
12 Fauchere, J.-L. and Petermann, C., Helv. Chim. Acta, 63 (1980) 824.
13 Kazlauskas, R.J., Trends Biotechnol., 12 (1994) 464, and references cited therein.
14 Cygler, M., Grochulski, P., Kazlauskas, R.J., Schrag, J.D., Bouthillier, F., Rubin, B., Serreqi, A.N. and Gupta, A.K., J. Am. Chem. Soc., 116 (1994) 3180.
15 Norin, M., Haeffner, F., Achour, A., Norin, T. and Hult, K., Protein Sci., 3 (1994) 1493.
16 Indy PC and Indigo II XL, Silicon Graphics Inc., Mountain View, CA, U.S.A.
17 QUANTA® (version 4.0), Molecular Simulations Inc., Waltham, MA, U.S.A.
18 Brooks, B.R., Bruccoleri, R.E., Olafson, B.D., States, D.J., Swaminathan, S. and Karplus, M., J. Comput. Chem., 4 (1983) 187.
19 CHARMm® (version 22.2), Molecular Simulations Inc., Waltham, MA, U.S.A.
20 Derewenda, U., Brozozowski, A.M., Lawson, D.M. and Derewenda, D.S., Biochemistry, 31 (1992) 1532.
21 Entry 4TGL of the PDB, version of July 1993.
22 a. Bernstein, F.C., Koetzle, T.F., Williams, G.J.B., Meyer Jr., E.F., Brice, M.D., Rodgers, J.R., Kennard, O., Shimanouchi, T. and Tasumi, M., J. Mol. Biol., 112 (1977) 535.
b. Abola, E., Bernstein, F.C., Bryant, S.H., Koetzle, T.F. and Weng, J., In Allen, F.H., Bergerhoff, G. and Sievers, R. (Eds.) Protein Data Bank in Crystallographic Databases – Information Content, Software Systems, Scientific Applications, Data Commission of the International Union of Crystallography, Bonn/Cambridge/Chester, 1987, pp. 107–132.